

INFLUENCE OF A TOOL'S ROTATIONAL SPEED ON THE MECHANICAL PROPERTIES OF FRICTION-STIR-WELDED JOINTS OF DISSIMILAR AA6082 AND AA5052 ALUMINIUM ALLOYS

VPLIV HITROSTI VRTENJA ORODJA NA MEHANSKE LASTNOSTI ZVARNIH SPOJEV IZ RAZLIČNIH ZLITIN NA OSNOVI ALUMINIJA, IZDELANIH Z VRTILNO-TORNIM POSTOPKOM VARJENJA

Ali Debih

Mechanical department, University of M'sila, M'sila, 28000, Algeria

Prejem rokopisa – received: 2024-07-06; sprejem za objavo – accepted for publication: 2024-08-28

doi:10.17222/mit.2024.1238

This study examines the influence of a tool's rotational speed on the microstructure and mechanical properties of dissimilar friction-stir-welded joints of AA6082 and AA5052 aluminium alloys. The joining process was carried out at various rotational speeds of 600 min⁻¹, 1000 min⁻¹, and 1400 min⁻¹ and a constant welding speed of 35 mm/min using a high-speed-steel (HSS-Co5) tool with a cylindrical pin. The microstructure of the welded joints was characterized using optical microscopy. The Vickers microhardness, tensile properties, and impact strength of welded joints were evaluated and compared to base metals. Results showed that the mechanical properties and the joint performance were considerably influenced by the tool's rotational speed due to the amount of heat input and the formation of macroscopic defects in the stir zone. It was found that a rotational speed of 1000 min⁻¹ is the suitable welding parameter for optimum mechanical properties. The welded joint at 1000 min⁻¹ shows a tensile strength of 122 MPa, elongation of 8.1 %, specific impact strength of 0.43 J/mm², and a maximum microhardness of 75 HV in the stir zone. In all welded joint samples, the fracture locations were near the edge of the welded zone on the retreating side. The results provide further insight into the appropriate selection of FSW process parameters that ensure excellent joints between AA5052 and AA6082 alloys with the required mechanical properties.

Keywords: aluminium alloys, friction stir welding, mechanical properties, microstructure

V članku avtor opisuje raziskavo vpliva parametrov hitrosti vrtenja orodja na mikrostrukturo in mehanske lastnosti zvarnih spojev med dvema različnima tipoma Al zlitin; to je AA6082 in AA5052. Zvarni spoji so bili izdelani s tako imenovanim vrtilno/mešalnim postopkom trenjskega varjenja (FSW; angl.: friction stir welding). Varjenje je bilo izvršeno pri različnih hitrostih vrtenja orodja 600 min⁻¹, 1000 min⁻¹ in 1400 min⁻¹. Hitrost varjenja je bila konstantna 35 mm/min in orodje je imelo cilindrično konico iz hitroreznega jekla vrse HSS-Co5. Za karakterizacijo mikrostrukture je avtor uporabil svetlobni metalografski mikroskop. Izmerjeno Vickersovo mikrotrdoto, natezne lastnosti in udarno žilavost je avtor primerjal z vrednostmi dobljenimi pri osnovnih dveh materialih. Rezultati preiskav in meritev so pokazali, da so na lastnosti zvarov močno vplivale različne hitrosti vrtenja orodja zaradi različnega vnosa toplote in tvorbe makroskopskih napak v conah vrtenja orodja. Avtor ugotavlja, da je hitrost vrtenja 1000 min⁻¹ najbolj primerna hitrost vrtenja orodja za doseganje optimalnih mehanskih lastnosti zvarov. Pri hitrosti 1000 min⁻¹ so bile v coni vrtenja orodja dosežene naslednje vrednosti: natezna trdnost 122 MPa, raztezek 8,1 %, specifična udarna žilavost 0,43 J/mm² in maksimalna Vickersova mikrotrdota 75 HV. Pri vseh preizkušancih je prišlo do njihovega loma na robu (blizu) cone varjenja po ponovni toplotni obdelavi. Avtor verjame, da predstavljeni dosežani rezultati preiskave omogočajo nadaljnjo pomoč pri izbiri parametrov FSW procesa varjenja, ki dajejo odličen zvarni spoj med zlitinama AA5052 in AA6082 z zahtevanimi mehanskimi lastnostmi.

Ključne besede: zlitine na osnovi aluminija, vrtilno/mešalni trenjski postopek varjenja, mehanske lastnosti, mikrostruktura

1 INTRODUCTION

Aluminium alloys are commonly used in many emerging fields such as automobile, aerospace, marine, and medical industries owing to their high strength-to-weight ratio and good formability.¹⁻⁷ For example, substituting steel with aluminium can result in a weight reduction of up to 40 %.^{1,4} However, aluminium alloys are often categorized as difficult to weld using fusion welding because of their high thermal conductivity, low melting point, affinity for oxygen and hydrogen, poor solidification microstructure, and porosity in the fusion zone.⁸⁻¹¹ While the production of aluminium components

is not very complex, the fusion welding of these alloys can present problems and challenges due to the excellent thermal and electrical conductivity, and the lack of structural transformation in the solid state.¹¹⁻¹³

Friction stir welding (FSW) is an innovative, solid-state welding technology that is widely used for both the similar and dissimilar joining of aluminium alloys. The FSW process has advantages over traditional fusion welding processes in terms of better mechanical properties, low residual stress, and reducing microstructural defects.^{8,9,14-16} Furthermore, FSW can be used in place of riveting on industrial components to save weight and production time, thus leading to a reduction in cost. The peculiarity of the FSW process is reflected in public health and the environment protection, as well

*Corresponding author's e-mail:
ali.debih@univ-msila.dz (Ali Debih)

Table 1: Chemical composition in weight percentage (w/%) of AA6082 and AA5052 BM

Alloy	Si	Cr	Mg	Mn	Ni	Cu	Zn	Fe	Al
AA6082	0.91	0.04	0.85	0.41	0.003	0.1	0.009	0.21	Balance
AA5052	0.17	0.11	2.31	0.08	0.02	0.09	0.03	0.23	Balance

as workplace safety, as it does not produce any harmful fumes, gases and radiation and is also safe for operators.^{5,17}

The FSW process uses a spinning, non-consumable cylindrical tool with a profiled pin and shaped shoulder to generate frictional heat in the joined piece.¹⁸ Heat is generated between the tool and material, and then mechanically intermixes the two pieces at the weld line, hence the softened metal, without reaching melting point, can be joined using mechanical pressure.^{19–23} The side where the rotational direction and the welding direction coincide is called the advancing side (AS), while the opposite side is defined as the retreating side (RS).

A complex microstructure, comprising the stir zone (SZ), heat-affected zone (HAZ), thermo-mechanically affected zone (TMAZ), and base metal (BM), is often created during FSW depending on the level of strain and the temperature cycle.^{1,24–27} In BM, the metal is characterized by no change in the structure and mechanical properties. In the HAZ, the material is only affected by the heat generated during welding. The TMAZ is characterized by a highly deformed microstructure since the material suffers from plastic deformation and insufficient heating for dynamic recrystallization (DRX). In the SZ, the metal that experiences both severe plastic deformation and high temperature leads to an excellent grain refinement owing to complete DRX process.

The strength and quality of the weld are typically determined by the heat produced and the material mixed during the welding process. Consequently, the FSW process parameters, including tool geometry, tool rotation speed, and axial load play a role in controlling the joint characteristics. Furthermore, the location of dissimilar base metals on the retreating or advancing sides affects the quality of the joint.^{18,26}

For industrial applications, the mechanical and physical characteristics of welded aluminium alloys are of primary importance. In this context, numerous research projects have studied the FSW of dissimilar Al alloys joints focusing on the effect of process parameters and process optimization.^{28–31} For instance, Kumbhar et al.²⁹ investigated the effect of the nugget zone microstructure on the mechanical properties of dissimilar FSW joints of AA5052-H32 and AA6061-T6 alloys. Their results showed that the inter-diffusion of alloying elements and the attainment of similar orientations in the nugget could have contributed to the good mechanical properties of the specimens. Lee et al.³⁰ investigated the effect of FSW parameters on the normal load and spindle torque during the welding of dissimilar AA5052-H112 and AA6061-T6 alloys. They found that the interface

morphologies were characterized by interface pull-up and pull-down on the advancing side and retreating side.

Although studies that have been published in the literature demonstrate that AA5052 and AA6082 alloys can be joined successfully using FSW technology, the kinematic parameters have a role in the FSW process. Hence in this investigation, an attempt was carried out in this area of research to understand the effect of rotational tool speed on the performance of FSW dissimilar AA6082 and AA5052 alloys. Three rotational speeds of 600 min⁻¹, 1000 min⁻¹ and 1400 min⁻¹ were used to obtain dissimilar AA6082 and AA5052 welds joints. Macrostructure, microstructure evolutions, microhardness, tensile and impact strength tests were carried out using an optical microscope, Vickers microhardness, tensile, and impact strength tests.

2 MATERIALS AND METHODS

The materials were rolled sheets of AA 6082 and AA 5052 aluminium alloys with 8 mm of thickness. The chemical compositions of the alloys are in **Table 1**.

The plates were slashed and milled into the required rectangular size of 150 mm × 50 mm × 8 mm, then grinded with abrasive paper of 1200 grit to achieve a superior surface finish. In the case of dissimilar butt joining, it has been demonstrated that better mechanical properties are obtained when harder material is placed on the advancing side (AS) and softer material is positioned on the retreating side (RS).^{18,26} Accordingly, the AA5052 plate was placed on the AS due to its higher mechanical strength, and the AA6082 plate was placed on the RS. The workpieces were arranged in a butt rectangular configuration, positioned in the fixture to avoid the separation of the plates during welding. The FSW was carried out using a universal milling machine (HURON). The welding tool used in this study was made of high-speed steel (HSS-Co5), which has high resistance to elevated temperatures. It has a cylindrical geometry with a shoulder diameter of 20 mm, and a pin diameter of 7 mm, while the length of the pin was 7.8 mm, as was the required welding depth of the plates with a tilt angle of 2°. Friction stir welds were carried out along the longitudinal direction of the plate at 600 min⁻¹, 1000 min⁻¹, and 1400 min⁻¹ as the tool's rotational speeds, keeping the constant traverse welding speed of 35 mm/min.

The microstructural observations were carried out using an optical microscope (*Olympus* A13.1031-B) with digital resolution at higher magnification. The samples for microstructural examination were prepared using Keller's reagent (180 mL distilled water + 2 mL HF + 2 mL HCl + 2 mL HNO₃).

Scanning electron microscopic observations (SEM) and energy-dispersive X-ray spectroscopy (EDS analysis) were performed using a JEOL-JSM 7001F microscope.

XRD analysis was conducted using an X'pert PRO diffractometer from PANalytical, equipped with Cu-K α radiation. X-ray measurements were performed at 35 kV and a current of 20 mA. The wavelength $\lambda_{K\alpha 1} = 0.15418$ nm was used for calculations. The general view of the X-ray patterns was taken with a scanning step of 0.02° in the range of 2θ angles from 10° to 90° . The X-ray patterns were analysed by X'Pert High Score plus and identified by the (Pcpdftwin database (JCPDS-ICDD) software.

The Vickers microhardness profiles were obtained on the longitudinal cross-section of each sample using a TUKON 2500 with a 0.5 N load for 15 s and a spacing of 0.5 mm along the mid-thickness line.

Samples for the tensile test were cut using an electro-discharge machine with dimensions of a gauge length of 25 mm, a thickness of 7 mm, and a gauge width of 6 mm. Tensile tests were performed at room temperature to fracture using a hydraulic testing machine at a strain rate of 10^{-3} s^{-1} . Three samples were tested for each rotational speed condition, with the averaged experimental data considered the final result.

Impact tests were conducted at room temperature on specimens having a length of 55 mm, width of 10 mm, and thickness of 7 mm using an impact-testing machine "Instron Wolpert" type with a maximum capacity of 300 J. For each rotational speed condition, at least three impact specimens were tested to determine the amount of energy absorbed during fracture and determine the specific impact toughness of the weld plates.

3 RESULTS AND DISCUSSION

3.1 Macrostructure and microstructure inspection

Figure 1 shows the top and root surface morphologies of the weld joints at 600 min^{-1} , 1000 min^{-1} , and

1400 min^{-1} , respectively. The welding directions, AS and RS are indicated in the same figure. A smooth weld and a good surface appearance are obtained with increasing the rotation speed due to the increase in heat input and material flow during stirring. A smooth weld and less surface appearance were obtained at the lowest value of rotation speed (600 min^{-1}) due to low temperature and low material flow, as shown in **Figure 1a**. The lower lateral flash was observed on the weld surface at a tool rotation speed of 1000 min^{-1} (**Figure 1b**). However, excessive lateral flash and grooves were observed on the retreating side (RS) of the butt joint, especially at the highest value of the tool rotation speed (1400 min^{-1}) resulting from the outflow of plasticized material from underneath the shoulder, as shown in **Figure 1c**. **Figures 1d–1f** show line defects as well as incomplete penetration on the root surfaces of the weld joints at all the welding rotational speeds. The occurrence of these defects indicates that a portion of the joint root is not completed and filled with weld metal. These defects reduce the quality of welding joints and impact the manufacturing cost of the workpieces.^{3,31–33}

Figure 2 presents the morphology of the cross-section of the welded joint at 600 min^{-1} , 1000 min^{-1} , and 1400 min^{-1} . The macroscopic defects appeared at the lowest (600 min^{-1}) and highest (1400 min^{-1}) tool rotational speeds. The formation of tunnel defect at the low tool rotation speed, as shown in **Figure 2a**, is probably caused by the inferior metal flow during the welding. While the groove defects observed in the weld joint at high tool rotation speed, as presented in **Figure 2c**, resulted from the outflow of the plasticized material from underneath the shoulder.

Joint strength decreases as the size of the tunnels and grooves increases. Joints having large grooving or tunnelling defects possessed lower mechanical properties and vice-versa. The cross-section of the welded joint at 1000 min^{-1} showed a typical FSW morphology without defects, for these reasons the samples welded at 1000 min^{-1} were chosen for the microstructural analysis.

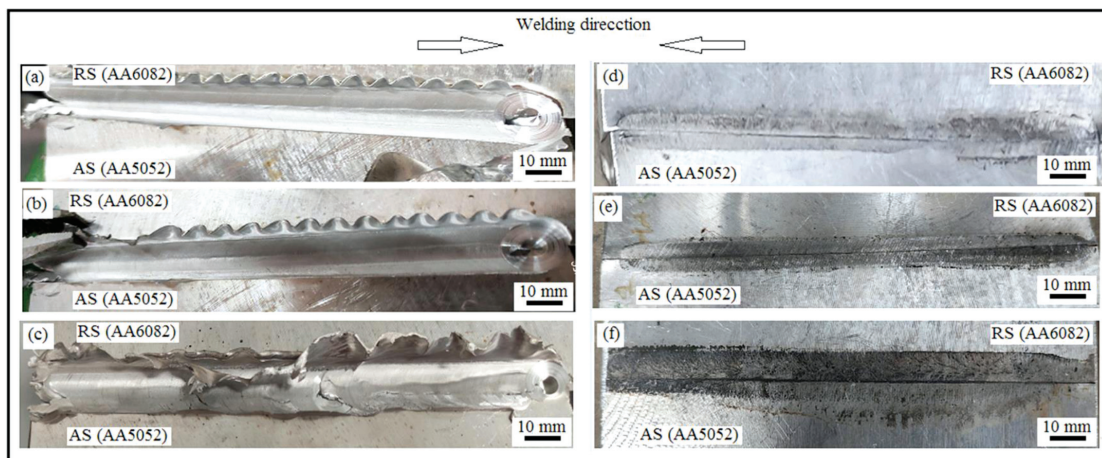


Figure 1: Top and root surface macrostructure of the weld joint at: a) and d) 600 min^{-1} , b) and e) 1000 min^{-1} , c) and f) 1400 min^{-1}

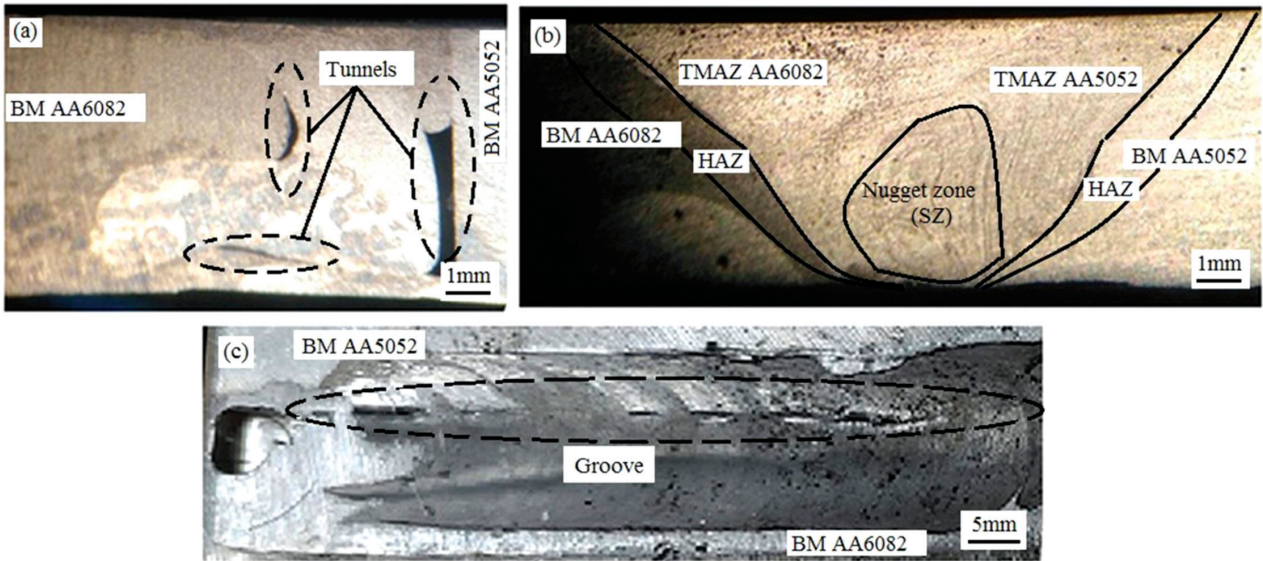


Figure 2: Cross-section morphology of the welds joint at: a) 600 min^{-1} , b) 1000 min^{-1} , and c) a groove-like defect revealed on the top surface of the weldment at 1400 min^{-1}

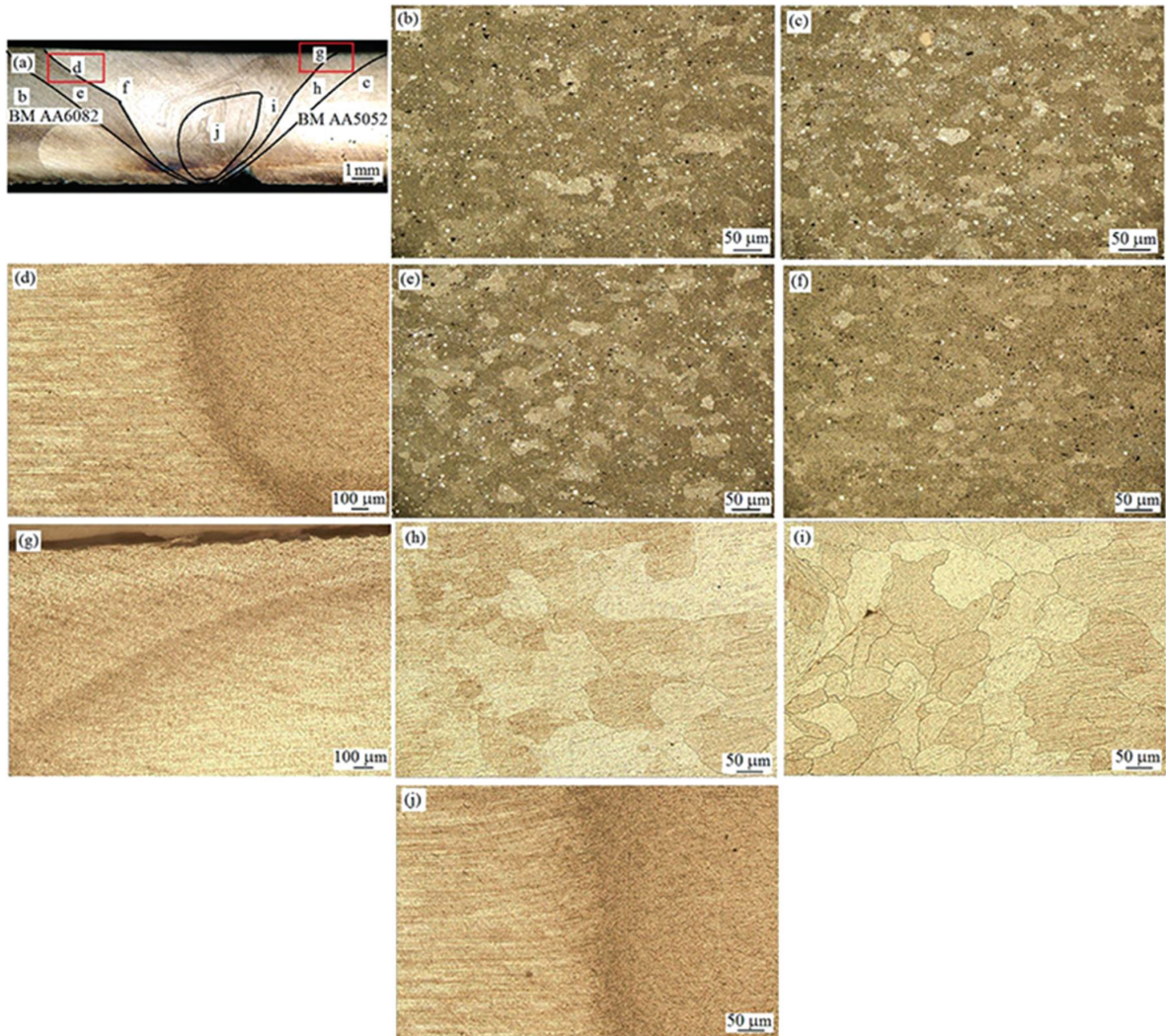


Figure 3: Microstructures of the different regions; a) regions of optical observations, b) 6082 base metal, c) 5052 base metal. d) Interface HAZ-TMAZ of 6082, e) TMAZ of 6082, f) TMAZ of 6082, g) interface HAZ-TMAZ of 5052, h) HAZ of 5052, i) TMAZ of 5052, j) Nugget zone

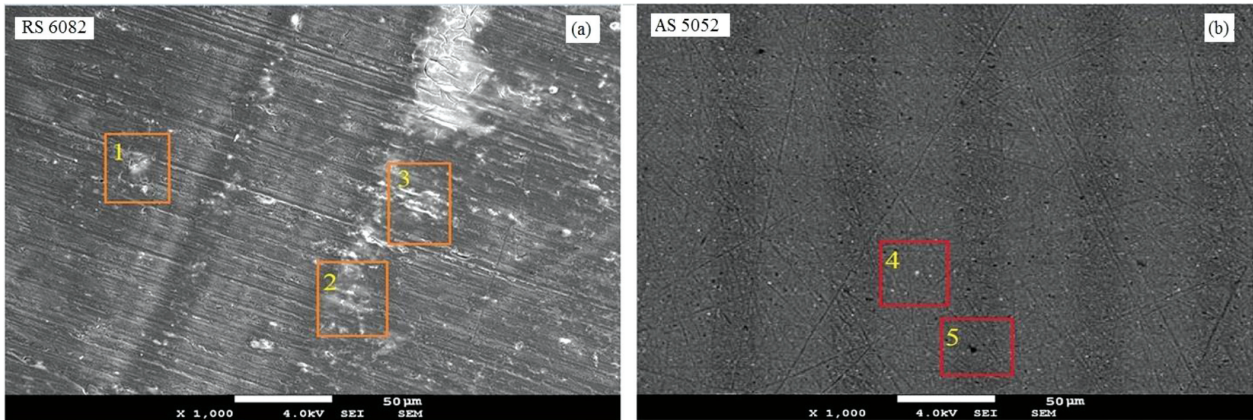


Figure 4: SEM micrographs in the NZ of dissimilar: a) AA 6082, b) AA 5052

Table 2: EDS analyses of the weld region microstructure (w/%)

Materials	Al	Mg	Si	Mn	Fe	Possible phase	
AA 6082	Spot 1	–	68.4	31.6	–	–	Mg ₂ Si
	Spot 2	62.21	1.3	13.2	0.19	23.1	β (AlFeSi)
	Spot 3	79.1	1.7	3.71	0.13	6.21	α Al(FeSi)
AA 5052	Spot 4	–	71.3	28.7	–	–	Mg ₂ Si
	Spot 5	81.65	–	–	–	18.35	Al ₆ Mn

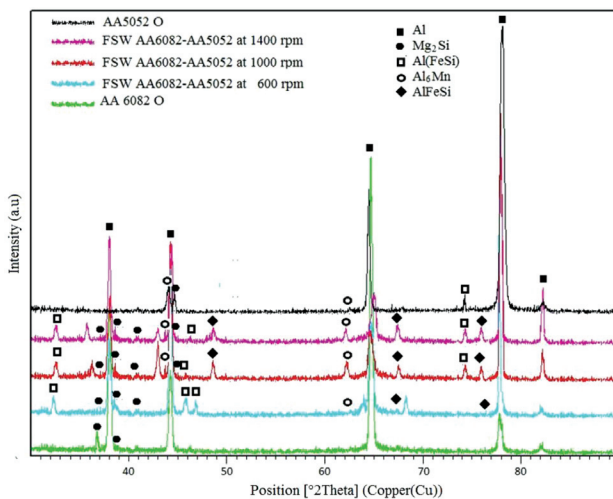


Figure 5: XRD spectra for base metals AA 6082, AA 5052 and NZ of FSW AA6082/AA5052 at different tool rotational speeds

As marked in **Figure 2b**, the weld joint at 1000 min⁻¹ is divided into four characteristic regions, BM, HAZ, TMAZ and the weld zone or SZ. More details on the microstructural characteristics of these regions are depicted in **Figure 3**.

The microstructures of AA 6082 and AA 5052 BM are shown in **Figures 3b** and **3c**, respectively. AA 6082 and AA 5052 alloys exhibit a typical rolled, deformed microstructure with elongated grains having average dimensions of 70 × 25 µm and 30 × 19 µm, respectively with the presence of second-phase particles along the rolling direction. SEM micrographs (**Figure 4**), EDS results (**Table 2**) and XRD pattern (**Figure 5**) indicated

that the second phases present in the AA5052 alloy were Mg₂Si and Al₆Mn phases. While the second phases identified in the AA6082 alloy were Mg₂Si and Al(FeSi) phases.

Figures 3d and **3g** depict distinguishable micrographs at the interfaces joint between the HAZ-TMAZ zones on the RS and AS, respectively. It is observed from **Figure 3e** that the microstructure of the HAZ on the RS becomes more equiaxed and refined with an average size of 40 µm than the AA6082 BM. It appears that the thermal cycle occurred in the HAZ help the recrystallization of rolled, deformed AA6082 BM. **Figure 3f** shows a typical microstructure of the TMAZ region of the RS, which is obviously more refined (26 µm) than that of the HAZ microstructure.

Figure 3h presents the microstructure of the HAZ on the AS, which is characterized by equiaxed grains but with large mean grain size of 100 µm. It is evident that the AA5052 alloy is more sensible to heat input than the AA6082 alloy. The microstructure of the TMAZ on the AS shown in **Figure 3i** exhibits more refined grains with a mean grain size of 50 µm than the HAZ due to high plastic strain induced by stirring. **Figure 3j** shows the microstructure of the SZ, which consists of extremely refined grains due to the occurrence of DRX. In this area, the AA6082 and AA5052 alloys were more thoroughly mixed than in the other regions.

3.2 Mechanical properties

We provide all the Vickers microhardness values for the base metals and the welded zones with a test load of 0.5 N and duration of 15 s. **Figure 6** shows the variation

of microhardness as a function of distance from the weld centre for the joints at 600 min⁻¹, 1000 min⁻¹, and 1400 min⁻¹. For comparison, the microhardness values of the AA 5052 (80 HV) and AA 6082 (35 HV) BM are displayed in the plot. The microhardness across the weld zones of all the samples is considerably lower than that of the AA5052 BM and comparatively higher than that of the AA6082 BM. It can be concluded that dissimilar joints present an intermediate behaviour.

In the SZ, the lowest microhardness value was recorded in the centre of the weld joint at 600 min⁻¹ (38 HV), 1000 min⁻¹ (57 HV) and 1400 min⁻¹ (55 HV). Then, the microhardness increases with increasing distance from the weld centre to reach a maximum of 56.8 HV at 3.5 mm from the weld centre at 600 min⁻¹, a 75 HV at -2 mm from the centre of the weld joint at 1000 min⁻¹, and 59.6 HV at -2.5 mm from the weld centre of the weld joint at 1400 min⁻¹, respectively. The rise in microhardness is attributed to the grain refinement and the formation of the second Mg₂Si and AlFeSi phases in the welding zone.

In the RS, the microhardness gradually decreases with increasing distance from the weld centre along the TMAZ and HAZ regions. It is interesting to note that the weld joint at 1000 min⁻¹ exhibits the highest microhardness values. The high microhardness values near the pin diameter can be attributed to the grain refinement caused by intensive stirring during the FSW. In contrast, the microhardness along the distance from the weld centre in the AS did not change with changing the tool rotational speed. The highly asymmetrical microhardness distribution along the cross-section of the welded joints was due to the different microstructural zones of both sides, which develop due to the thermo-mechanical history during elaboration and welding.

Figure 7 presents the stress-strain curves of the BM and weld joints at 600 min⁻¹, 1000 min⁻¹, and

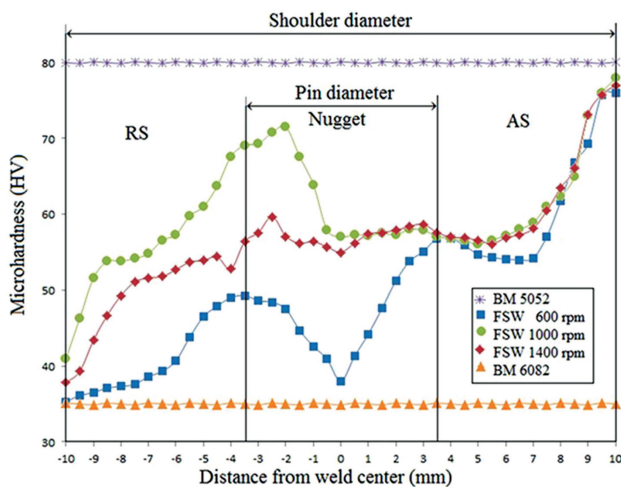


Figure 6: Microhardness evolution as a function of distance from the weld centre for the weld joint at 600 min⁻¹, 1000 min⁻¹, and 1400 min⁻¹. The microhardnesses of AA6082 and AA5052 BM are given for comparison.

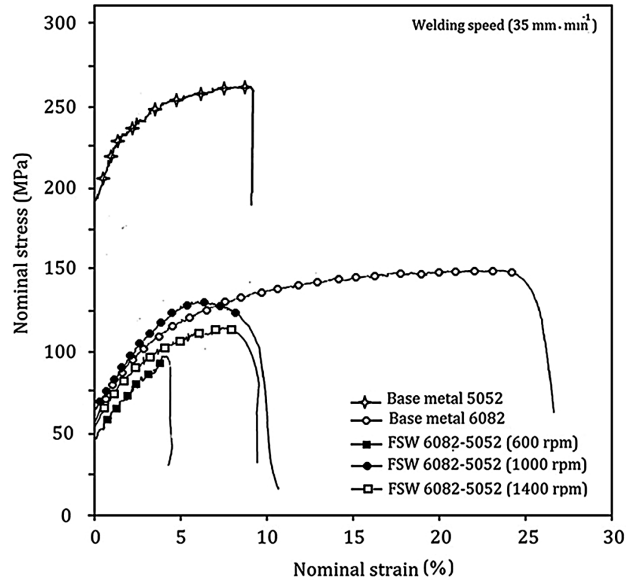


Figure 7: Stress-strain curves for AA 6082, AA 5052 BM and weld joint at 600 min⁻¹, 1000 min⁻¹ and 1400 min⁻¹

1400 min⁻¹. Table 3 summarizes the tensile properties including the tensile strength (UTS), 0.2 % yield strength (YS), elongation at break (A %), and joint efficiency (%). The joint efficiency is calculated based on the FSW joint strength relative to the strength of the base metals. Additionally, micrographs showing the failure locations of tensile specimens after testing are presented in Figure 8. The results demonstrate that the tensile properties of the welded joints fluctuated with respect to different rotational speeds. The AA5052 BM alloy presents a higher yield strength and a higher tensile strength, but a lower percentage of elongation. For the welded specimens, it was found that dissimilar joints obtained at 1000 min⁻¹ exhibited good tensile properties. In contrast, joints obtained at 600 min⁻¹ and 1400 min⁻¹ showed lower strengths compared to AA6082 and AA5052 BM. It is interesting to note that all the joints fractured near the weld edge in the HAZ-TMAZ zone along the RS, as shown in Figure 8. This was due to the lower yield

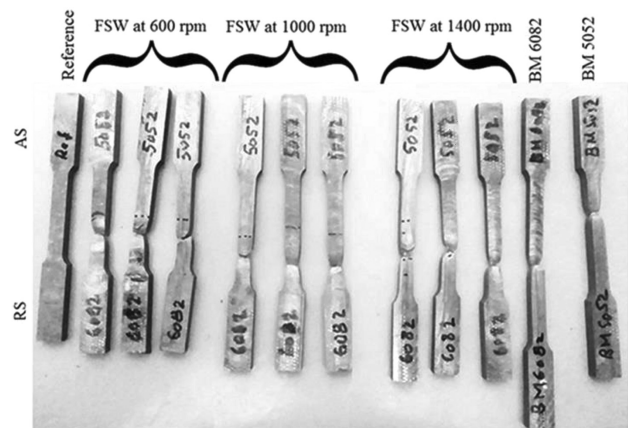


Figure 8: Failure locations of transverse tensile specimens

Table 3: Tensile test results and specific impact energy values of AA 6082 and AA 5052 welded specimens

Condition	UTS, MPa	YS, MPa	A, %	Joint efficiency, %	Specific impact energy, (J/mm ²)
AA6082 BM	127	59	27	–	0.71
AA5052 BM	265	194	9.7	–	0.32
FSW at 600 min ⁻¹	95	47	3.4	36–75	0.49
FSW at 1000 min ⁻¹	122	57	8.1	46–96	0.43
FSW at 1400 min ⁻¹	111	55	8.7	41–87	0.19

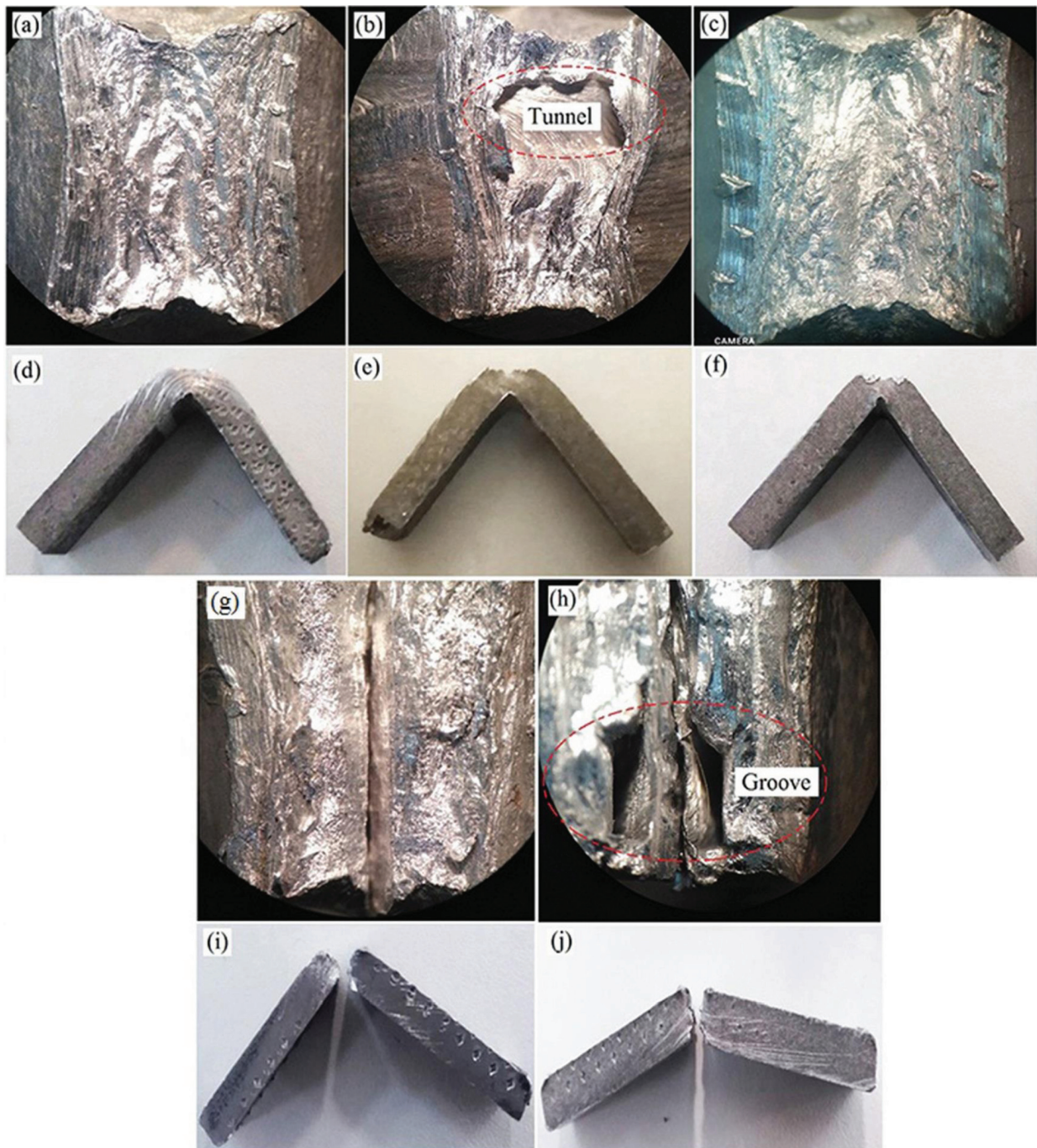


Figure 9: Impact energy fracture surface of specimens. a) base metal 6082, b) FSW at 600 min⁻¹, c) FSW at 1000 min⁻¹, d) lateral view of the base metal 6082 impact specimen, e) lateral view of the FSW specimen at 600 min⁻¹, f) lateral view of the FSW specimen at 1000 min⁻¹, g) fracture surface of base metal 5052, h) FSW at 1400 min⁻¹, i) lateral view of the base metal 5052 impact specimen and j) lateral view of the FSW specimen at 1400 min⁻¹

strength of the AA6082 alloy compared to the AA5052 alloy in the AS.

The welded joint at 600 min⁻¹ exhibits the lowest tensile strength and ductility of 95 MPa and 3.4 %, respectively. This reveals that the heat generated by the welding at 600 min⁻¹ was insufficient to plasticize the metals, leading to the formation of tunnel and void defects. The welded joint at 1000 min⁻¹ had a tensile strength of 122 MPa and an elongation to failure of 8.1 %. The improvement in the mechanical properties is a consequence of the microstructural evolution. Indeed, the microstructural examination of the weld joint at 1000 min⁻¹ showed that the SZ exhibits a refined grains structure without defects in which the AA5052 and the AA6082 metals were properly mixed. The tensile strength of the welded joint at 1400 min⁻¹ decreased to 111 MPa, but showed good ductility (8.7 %). This reveals that the friction generated by the tool produces excessive heat, making the metal too plastic, resulting in good ductility, but also producing excessive grooves and lateral flash, as shown in **Figures 1** and **2**. This happened due to the improper mixing of the metals in the welded zone.

The tensile properties of the joints are affected by the welding rotation speed, and they are very close to the AA6082 BM on the RS. The ultimate strength efficiency for the 5052–6082 joints, produced at 600 min⁻¹, 1000 min⁻¹, and 1400 min⁻¹, was 75 %, 96 %, and 87 % compared to the base metal AA 6082 alloy. Specimens of base metal 5052 present the lowest ductility compared to that of AA 6082, with 10 % as a percentage of elongation. The ductility is reduced by 17 % for the specimens welded at 1000 min⁻¹. The percentage of elongation of specimens processed at 1400 min⁻¹ is observed to be 8.7 %, whereas only 3.4 % of elongation is observed for specimens processed at 600 min⁻¹. It can be determined from the relation between the tensile properties and welding parameters that the rotation speed and welding speed designed at 1000 min⁻¹ and 35 mm/min are optimum for the ultimate strength.

The specific impact energy values of AA6082 BM, AA5052 BM, and welded joint at 600 min⁻¹, 1000 min⁻¹, and 1400 min⁻¹ are given in **Table 3**. The specific impact energy decreased from 0.49 J/mm² to 0.19 J/mm² when the rotational tool speed increased from 600 min⁻¹ to 1400 min⁻¹. The loss in specific impact energy at high rotational tool speed may be due to high heat input, resulting in a coarse-grained structure, the presence of defects and improper bonding in the welded zone. The lateral view and appearance of the fracture surface of the samples after the impact strength test are shown in **Figure 9**. The lateral view of AA6082 BM, weld joint at 600 min⁻¹ and 1000 min⁻¹ demonstrated that these samples did not break after the impact-strength test, revealing that the FSW joint did not lose its ductility (**Figures 9a–9c**). The fracture surface appearance of AA6082 BM exhibits a typical shear lips morphology, which is a characteristic of ductile material. A tunnel is visible in the fracture surface appearance of weld joint sample at

600 min⁻¹, (**Figure 9b**). While the surface appearance of the sample weld joint at 1000 min⁻¹ is smoother. **Figures 9g–9j** show that the AA5052 BM and the weld joint at 1400 min⁻¹ fractured after the impact strength test. Since the AA5052 BM is a brittle alloy, its fracture surface appeared as a flat smooth fracture, while grooves are visible in the fracture surface of the weld joint at 1400 min⁻¹, as shown in **Figure 9h**.

4 CONCLUSIONS

The present work investigated the impact of a tool's rotational speed on the mechanical properties of the FSW dissimilar AA 5052 and AA6082 alloys. From the experimental results, the following conclusions are drawn:

- The joint of dissimilar AA 5052 and AA6082 alloys was successfully performed using FSW processing at tool rotational speeds of 600 min⁻¹, 1000 min⁻¹ and 1400 min⁻¹ and a constant welding speed of 35 mm/min using a cylindrical pin.
- Due to insufficient and excess heat input, tunnel and groove defects developed in the weld joints at 600 min⁻¹ and 1400 min⁻¹, respectively. In contrast, FSW at 1000 min⁻¹ produced a defect-free weld joint composed mainly of SZ, TMAZ, HAZ and BM.
- The microhardness distribution along the cross-section of the welded joints was highly asymmetrical due to the microstructural heterogeneity produced during FSW and the dissimilar AA 5052 and AA6082 BM alloys. The microhardness in the centre of the stir zone was found around 38 HV at 600 min⁻¹, 57 HV at 1000 min⁻¹, 55 HV at 1400 min⁻¹.
- Optimum mechanical properties were obtained during FSW with a rotational speed of 1000 min⁻¹. The welded joint at 1000 min⁻¹ shows a tensile strength of 122 MPa, elongation of 8.1 %, and specific impact strength of 0.43 J/mm².
- The fractures of all the weld-joint samples during the tensile test were located on the retreating side at the softest points of the HAZ-TMAZ zone.

5 REFERENCES

- ¹ R. Vijayakumar, V. Kannan, A. Natarajan, Aluminium Alloys - Recent Trends in Processing, Characterization, Mechanical Behavior and Applications, INTECH, USA 2017, 81, doi:10.5772/intechopen.70233
- ² K. V. P. Chandu, E. V. Rao, A. S. Rao, B. V. Subramanyam, The Strength of Friction Stir Welded Aluminium Alloy 6061, Int. j. res. mech. eng. technol., 4 (2014)1, 119-122
- ³ J. Adamowski, M. Szkodo, Friction Stir Welds (FSW) of aluminium alloy AW6082-T6, J. Achiev. Mater. Manuf., 20 (2007)1-2, 403-406.
- ⁴ A. Pandey, A. S. Khan, E. Y. Kim, S. H. Choi, T. Gnäupel-Herold, Experimental and numerical investigations of yield surface, texture, and deformation mechanisms in AA5754 over low to high temperatures and strain rates, Int. J. Plast., 41(2013), 165-188, doi:10.1016/j.ijplas.2012.09.006

- ⁵ N. Z. Khan, A. N. Siddiquee, Z. A. Khan, Friction Stir Welding: Dissimilar Aluminum Alloys, CRC Press, USA, 2017.
- ⁶ D. Kumar, S. S. Kumar, Investigation of mechanical behavior of friction stir welded joints of AA6063 with AA5083 aluminum alloys, *Mech. Mech. Eng.*, **23**(2019), 59-63, doi:10.2478/mme-2019-0008
- ⁷ B. Stojanovic, M. Bukvic, I. Epler, Application of Aluminum and Aluminum Alloys in Engineering, *Appl. Eng. Lett.*, **3** (2018)2, 52-62, doi:10.18485/aletters.2018.3.2.2
- ⁸ G. Mathers, The welding of aluminium and its alloys, CRC Press, USA, 2002
- ⁹ M. Perovic, D. Veljic, M. Rakin, N. Radovic, A. Sedmak, N. Bajic, Friction-stir welding of high-strength aluminium alloys and a numerical simulation of the plunge stage, *Mater. Tehnol.*, **46** (2012)3, 215–221
- ¹⁰ C. Vimalraj, P. Kah, Experimental Review on Friction Stir Welding of Aluminium Alloys with Nanoparticles, *Metals*, **11** (2021) 390, doi:10.3390/met11030390
- ¹¹ S. J. Doshi, A. V. Gohil, N.D. Mehta, S.R. Vaghasiya, Challenges in Fusion Welding of Al alloy for Body in White, *Mater. Today Proc.*, **5** (2018) 2, 6370–6375. doi:10.1016/j.matpr.2017.12.247
- ¹² P. Kah, R. Rajan, J. Martikainen, R. Suoranta, Investigation of weld defects in friction-stir welding and fusion welding of aluminium alloys, *Int. j. mech. mater. eng. Int. j. mech. mater. eng.*, **26** (2015), 1–10, doi:10.1186/s40712-015-0053-8
- ¹³ K. Martinsen, S. J. Hu, B. E. Carlson, Joining of dissimilar materials, *CIRP Ann. - Manuf. Technol.*, **64** (2015), 679–699, doi:10.1016/j.cirp.2015.05.006
- ¹⁴ V. Bhojak, J. K. Jain, K. K. Saxena, B. Singh, K. A. Mohammed, Friction Stir Process: A Comprehensive Review on Material and Methodology, *Indian J. Eng. Mater. Sci.*, **30** (2023), 45–64, doi:10.56042/ijems.v1i1.61877
- ¹⁵ B. Singh, A. Sankhla, K. K. Saxena, P. Singhal, Mechanical and Microstructural Evolution of Friction Stir Welded Joint of AA2014 Alloys, *Indian J. Eng. Mater. Sci.*, **29** (2022), 598-604, doi:10.56042/ijems.v29i5.67616
- ¹⁶ S. Jannet, P. K. Mathews, R. Raja, Comparative investigation of friction stir welding and fusion welding of 6061 T6 – 5083 O aluminum alloy based on mechanical properties and microstructure, *Bull. Pol. Acad. Sci. Tech. Sci.*, **62** (2014)4, 791-995, doi:10.2478/bpasts-2014-0086
- ¹⁷ S. Yazdaniyan, Z. W. Chen, Effect of friction stir lap welding conditions on joint strength of aluminium alloy 6060, *IOP Conf. Ser. Mater. Sci. Eng.* **4** (2009) 012021, doi:10.1088/1757-899X/4/1/012021
- ¹⁸ M. W. Safeen, P. R. Spena, Main Issues in Quality of Friction Stir Welding Joints of Aluminum Alloy and Steel Sheets, *Metals*, **9** (2019) 610, doi:10.3390/met9050610
- ¹⁹ P. H. Bindu, M. Mallampati, A. R. Rao, Design and Thermal Analysis of Welding Tools, *Int. j. innov. res. sci. eng. technol.*, **7**(2018) 7, 8055–8059, doi:10.15680/IJRSET.2018.70707073
- ²⁰ A. Kubit, R. Kluz, K. Ochalek, D. Wydrzyński, T. Trzepieciński, Friction stir welding of 2024-T3 aluminium alloy sheet with sheet pre-heating, *Mater. Tehnol.*, **52**(2018) 3, 283–288, doi:10.17222/mit.2017.084
- ²¹ M. T. S. M. Said, D. A. Hamid, A. Ismail, S. N. N. Zainal, M. Awang, M. A. Rojan, I. M. Ikram, M. F. Makhtar, Experimental Study on Effect of Welding Parameters of Friction Stir Welding (FSW) on Aluminium AA5083 T-joint, *Inform. Technol. J.*, **15**(2016), 99–107, doi:10.3923/ijtj.2016.99.107
- ²² C. Elanchezhian, B. V. Ramnath, P. Venkatesan, S. Sathish, T. Vignesh, R.V. Siddharth, B. Vinay, K. Gopinath, Parameter Optimization of Friction Stir Welding Of AA8011-6062 Using Mathematical Method, *Procedia Eng.*, **97** (2014), 775–782, doi:10.1016/j.proeng.2014.12.308
- ²³ A. Şık, A. Özer, The Effects of Friction Stir Welding Parameters on Microstructure, Fatigue Life and Tensile Properties of Aluminum 2024-T3 Alloy, *Arch. Metall. Mater.* **68** (2023) 2, 499–505, doi:10.24425/amm.2023.142428
- ²⁴ R. Kumar, A. Ghosh, S. Chattopadhyaya, Emerging Friction Stir Welding for Aluminium and its Applications, *Journal of Manufacturing and industrial engineering*, **2** (2014), 1–5, doi:10.12776/mie.v14i1-2.460
- ²⁵ H. S. Patil, S. N. Soman, Experimental study on the effect of welding speed and tool pin profiles on AA6082-O aluminium friction stir welded butt joints, *Int. J. Eng. Sci. Tech.*, **2**(2010) 5, 268–275, doi:10.4314/ijest.v2i5.60163
- ²⁶ P. Sadeesh, M. V. Kannan, V. Rajkumar, P. Avinash, N. Arivazhagan, K. D. Ramkumar, S. Narayanan, Studies on Friction Stir Welding of AA 2024 and AA 6061 Dissimilar Metals, *Procedia Eng.*, **75** (2014), 145–149, doi:10.1016/j.proeng.2013.11.031
- ²⁷ I. I. Marhoon, A. K. Al-Kamal, M. A. Abdulrehman, Studying the Mechanical Properties for 5086 Aluminum Alloy Welded Plates by Friction Stir Welding (FSW), *IOP Conf. Ser. Mater. Sci. Eng.*, **454** (2018) 012084, doi:10.1088/1757-899X/454/1/012084
- ²⁸ A. Sasikumar, S. Gopi, D. G. Mohan, Effect of welding speed on mechanical properties and corrosion resistance rates of filler induced friction stir welded AA6082 and AA5052 joints, *Mater. Res. Express*, **8** (2021) 6, 1–12, doi:10.1088/2053-1591/ac0c9e
- ²⁹ N. T. Kumbhar, K. Bhanumurthy, Friction Stir Welding of Al 5052 with Al 6061 Alloys, *Journal of Metallurgy*, (2012), 1–7, doi:10.1155/2012/303756
- ³⁰ C. Y. Lee, W. B. Lee, J. W. Kim, D. H. Choi, Y. M. Yeon, S. B. Jung, Lap joint properties of FSWed dissimilar formed 5052 Al and 6061 Al alloys with different thickness, *J. Mater. Sci.*, **43** (2008), 3296–3304, doi:10.1007/s10853-008-2525-1
- ³¹ V. Patel, W. Li, G. Wang, F. Wang, A. Vairis, P. Niu, Friction Stir Welding of Dissimilar Aluminum Alloy Combinations: State-of-the-Art, *Metals*, **9**(2019), 1–19, doi:10.3390/met9030270
- ³² I. Shigematsu, Y. J. Kwon, K. Suzuki, T. Imai, N. Saito, Joining of 5083 and 6061 aluminum alloys by friction stir welding, *J. Mater. Sci. Lett.*, **22**(2003) 5, 353–356
- ³³ H. R. Ghazvinloo, A. H. Raouf, N. Shadfar, Influence of Friction Stir Welding Variables on Surface Appearance of Joints Produced in SSM Cast A356 Aluminum Alloy, *J. Mater. Environ. Sci.*, **12**(2021)9, 1158–1164